Supporting Information

Kinetic analysis

The dynamic parameters in the kinetic model were optimized in Matlab 2016a from experimental data. The complete reaction paths for the dehydration of xylose and glucose contain a series of coupled ordinary differential equations, in which the reaction rate constants are associated with temperature through the Arrhenius formula. Under various reaction conditions, several completed sets of concentration data for reactants and products were used to solve the nonhomogeneous linear differential equations in the reaction model by the ode15s function, which is a rigid solver based on the numerical differential formula. Simultaneously, the lsqnonlin function based on least square method was used to perform nonlinear fitting of the solution results to obtain the optimal dynamic parameter prediction values.

AlPO$_4$ formation

Phosphate acid will be transformed into insoluble metal phosphate in carbon-based catalysts, which can promote a bond breaking reaction of the precursor matrix, and the formation of phosphate bonds like phosphate and polyphosphate. Phosphate bonds are strongly binded to the particles, leading to complete structural transition.[1] For example, Y. Takita et al.[2] obtained AlPO$_4$ by co-precipitation of aluminum nitrate and phosphate acid, which proved that metal phosphate was facile to form in the preparation environment of high-temperature pyrolysis as the metal salt mixed with phosphoric acid. M. Khabbouchi et al.[3] mixed phosphate acid with kaolin, and found that AlPO$_4$ was formed by pyrolysis at 250°C, 500°C ,750°C and 1000°C. Furthermore, R. Li et al.[4] and L. Zhang et al.[5] also demonstrated that AlPO$_4$ could be formed using aluminum lactic acid and either phosphate acid or subphosphate acid. It is seen that AlPO$_4$ can be formed in a mild environment where phosphoric acid is mixed with aluminum-containing substances. The aluminum-containing precursor Al(NO$_3$)$_3$·9H$_2$O and phosphate used in the present study are very similar to those of L. Zhang, and the results of XRD, TEM-EDS, FTIR and XPS show that the Lewis acidic active component formed on the surface of the catalyst is indeed the AlPO$_4$.[5]

Column chromatography

As for column chromatography, the insoluble matrix is first filled in the cylindrical tube to form a fixed phase. The sample is added to the column and washed off with a special solvent (0.005M H$_2$SO$_4$), which forms the flow phase. During the removal of the sample from the column, the distribution coefficient of different components in the fixed phase (adsorbent) and flow phase (0.005M H$_2$SO$_4$) are different. In general, the elongated columns favor material separation, but for a long separation time. The column used is a BioRad HPX-87H (7.8 mm × 300 mm). The total test time is 60 min, and the retention time of glucose, xylose, HMF, LA, and FF is 9.55, 10.80, 29.93, 15.09, and 45.23 min, respectively.

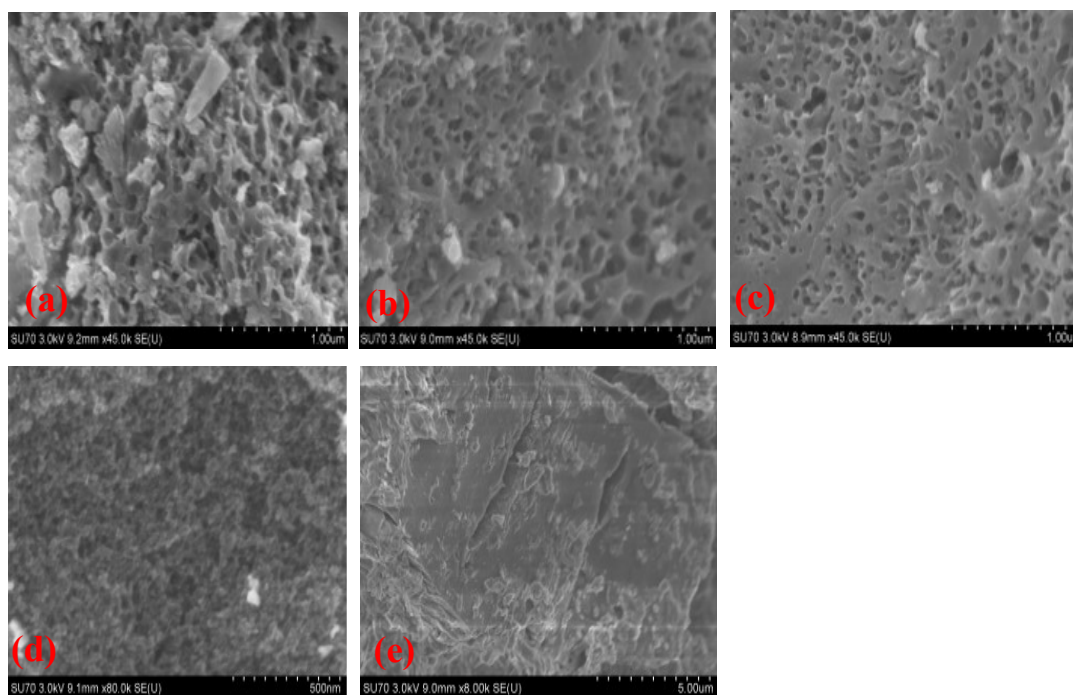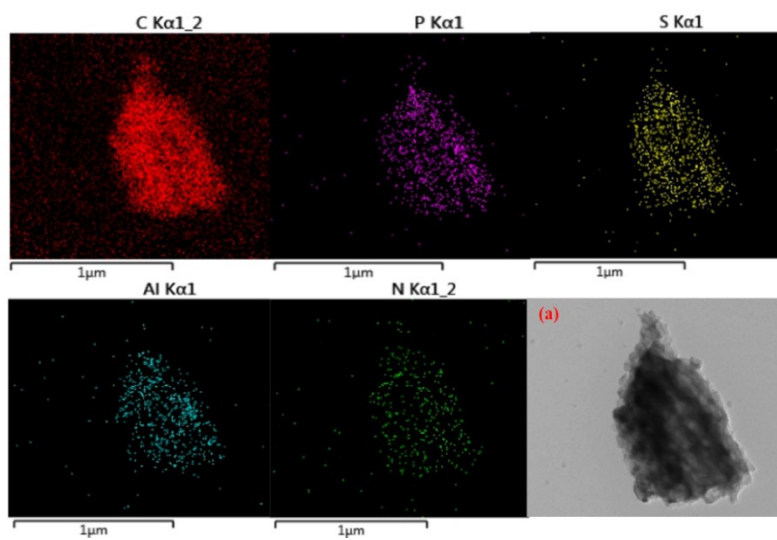**Catalyst characterization**

Fig. S1 SEM of catalyst (a) fresh DFCSA-P, N, Al catalyst; (b) DFCSA-P, N, Al after hydrolysis of glucose; (c) DFCSA-P, N, Al after hydrolysis of xylose (170 °C, 2 h, 0.05 g catalyst, 0.1 g sugar); (d) DFCSA-P, Al; (e) DFCSA-N, Al.
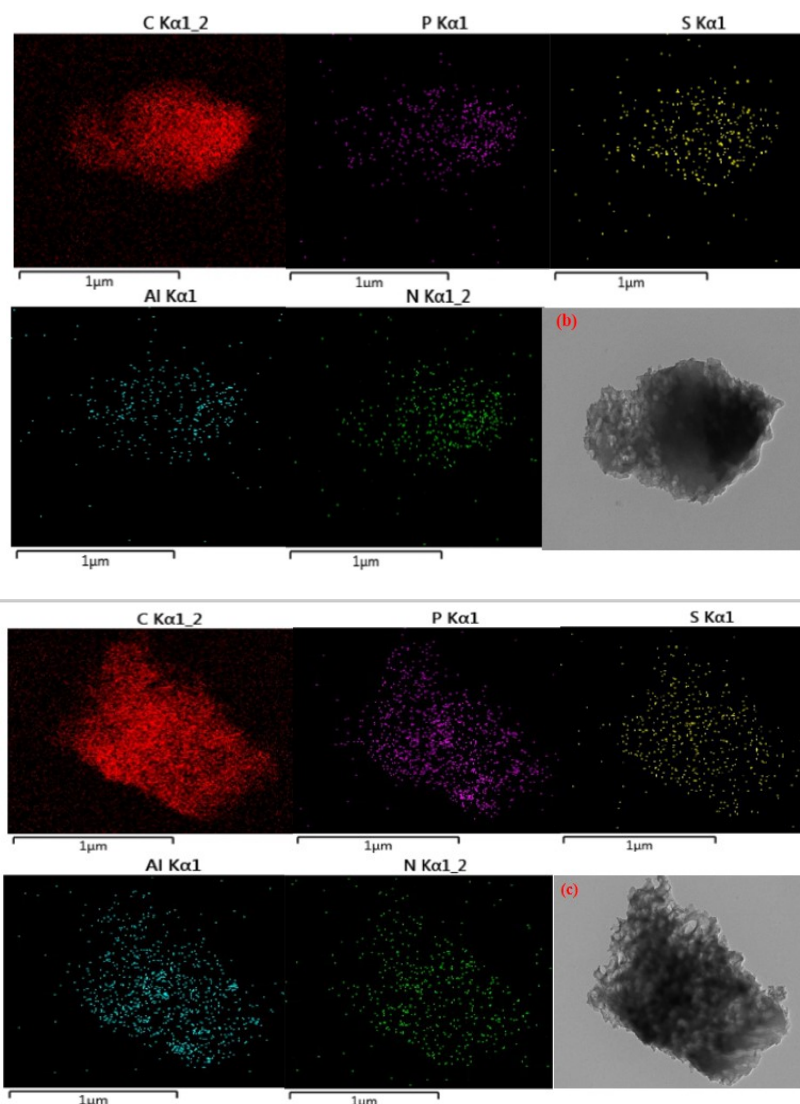
Fig. S2 TEM-EDS of (a) fresh DFCSA-P, N, Al catalyst. (b) DFCSA-P, N, Al after hydrolysis of glucose. (c) DFCSA-P, N, Al after hydrolysis of xylose.
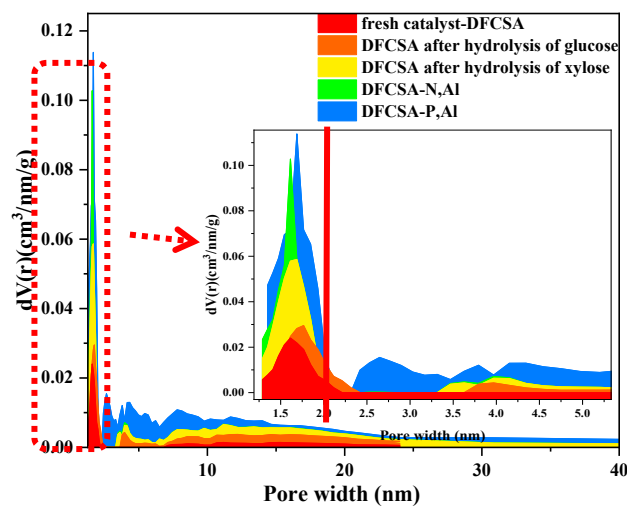

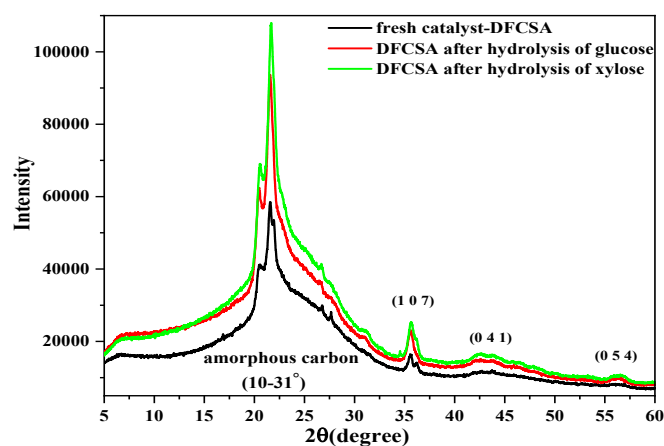**Fig. S3** Pore size and pore volume distribution of catalyst.
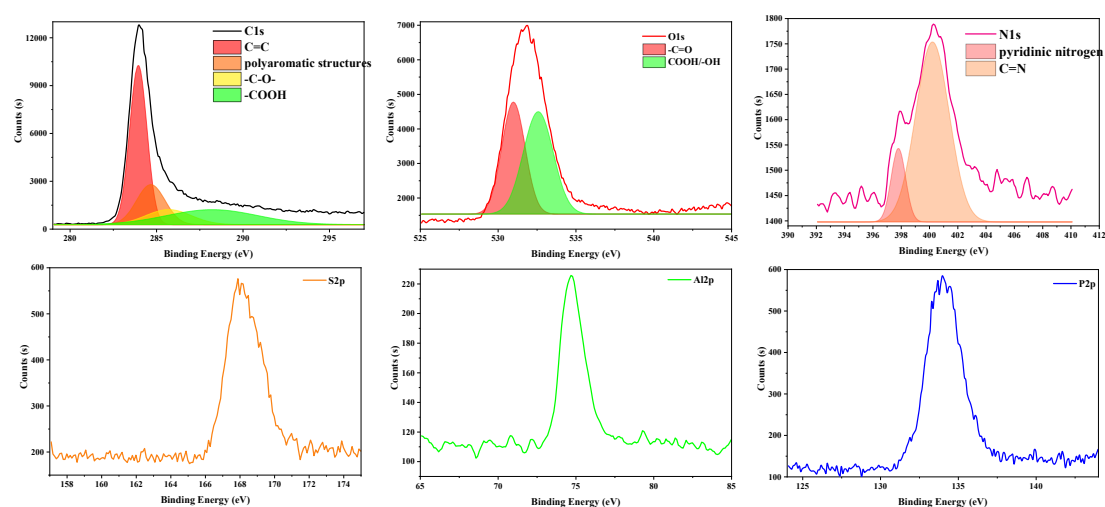
Fig. S4 XRD patterns of catalysts.

Fig. S5 X-ray photoelectron spectroscopy (XPS) patterns of the catalyst.

Table S1 Functional groups on the catalyst from XPS patterns.

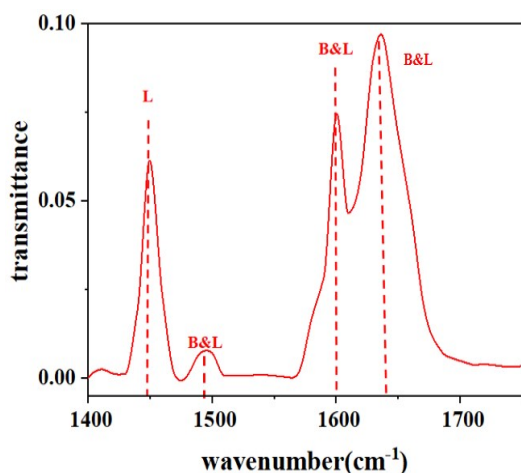| Groups	Binding energy (eV)	Element	Ref	Groups	Binding energy (eV)	Element	Ref
C-O-	283.86		6	C=N	400		9
C=C	283.3		7	pyridinic nitrogen	398.3	N1s	12
COOH	288.8	C1s	7	SO_{2-4}	168.7	S2p	10
Polyaromatic structure	284.6		8	$AlPO_4$	75	Al2p	11
C=O	531.1		8	$AlPO_4$	134.2	P2p	11
-COOH/-OH	532.3	O1s	8				

Fig. S6 Pyridine infrared spectrum of catalyst.
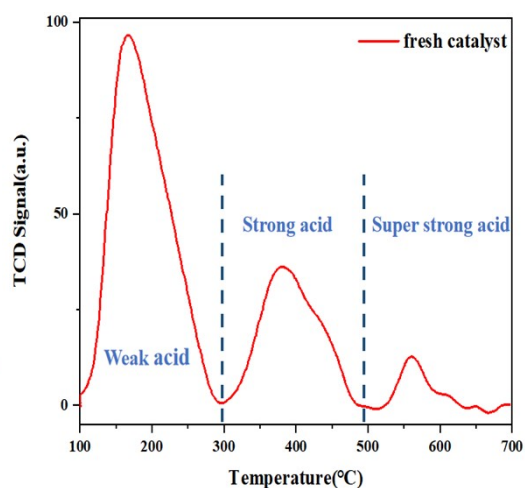
Fig. S7 NH$_3$-TPD patterns of catalysts.

Table S2 Quantitative results of infrared pyridine spectrum and NH3-TPD.

IR-FTIR		NH$_3$-TPD	
B(1422cm^{-1})/μmol·g^{-1}	60.69	Weak (100-300 °C)/μmol·g^{-1}	403.07
B&L(1486cm^{-1})/μmol·g^{-1}	2.13	Strong (300-500 °C)/μmol·g^{-1}	157.94
B&L(1611&1638cm^{-1})/μmol·g^{-1}	322.16	Super strong (>500 °C)/μmol·g^{-1}	23.34

Rrference

1 C. Lim. C. Srinivasakannan and A. Al Shoaibi. *Journal of Cleaner Production*. 2015, **102**, 501.

2 Y. Takita. H. Wakamatsu and G. Li. *Journal of molecular catalysis. A, Chemical*. 2000, **155(1-2)**, 111.

3 M. Khabbouchi. K. Hosni and M. Mezni. *Applied clay science*. 2017, **146**, 510.

4 R. Li. Y. Fan and B. Tang. *Materials chemistry and physics*. 2011, **125(1-2)**, 87.

5 L. Zhang. H. Eckert and G. Helsch. *Zeitschrift für physikalische Chemie (Neue Folge)*. 2005, **219(1)**, 71.

6 H. Chu. X. Guo and J. Liang. *Science China. Chemistry*. 2010, **53(4)**, 846.

7 K. Sa. C. Mahakul and B. Das. *Materials letters*. 2018, **211**, 335.

8 Y. Chiang. W. Lin and Y. Chang. *Applied surface science*. 2011, **257(6)**, 2401.

9 E. Touzé. F. Gohier and B. Daffos. *Electrochimica acta*. 2018, **265**, 121.

10 B. Tan. S. Zhan and W. Li. *Journal of industrial and engineering chemistry (Seoul, Korea)*. 2019, **77**, 449.

11 T. Appapillai. N. Mansour and J. Cho. *Nanoparticle Coating: Combined STEM and XPS Studies*. 2007, **19(23)**, 5748.

12 A. Benyounes. F. Ouanj and S. Louisia. *Catalysis today.* 2018, **301**, 183.